High bandwidth optical force clamp for investigation of molecular motor motion

Subhrajit Roychowdhury, Tanuj Aggarwal, Srinivasa Salapaka, and Murti V. Salapaka

Citation: Applied Physics Letters **103**, 153703 (2013); doi: 10.1063/1.4824816
View online: http://dx.doi.org/10.1063/1.4824816
View Table of Contents: http://scitation.aip.org/content/aip/journal/apl/103/15?ver=pdfcov
Published by the AIP Publishing

APPLIED PHYSICS LETTERS **103**, 153703 (2013)

High bandwidth optical force clamp for investigation of molecular motor motion

Subhrajit Roychowdhury,[1] Tanuj Aggarwal,[2] Srinivasa Salapaka,[3] and Murti V. Salapaka[4,a)]
[1]*Department of Electrical and Computer Engineering, University of Minnesota-Twin Cities, 2-270 Keller Hall, Minneapolis, Minnesota 55455, USA*
[2]*Cymer Inc., 17075 Thornmint Ct, San Diego, California 92127, USA*
[3]*Department of Mechanical Science and Engineering, University of Illinois at Urbana-Champaign, 362C Mechanical Engineering Bldg., 1206 W. Green St., Urbana, Illinois 61801, USA*
[4]*Department of Electrical and Computer Engineering, University of Minnesota-Twin Cities, 5-161 Keller Hall, Minneapolis, Minnesota 55455, USA*

(Received 24 April 2013; accepted 20 September 2013; published online 10 October 2013)

Use of optical tweezers for load force regulation on processive motors has yielded significant insights into intracellular transport mechanisms. The methodology developed in this letter circumvents the limitations of existing active force clamps with the use of experimentally determined models for various components of the optical tweezing system, thus making it possible to probe motor proteins at higher speeds. This paradigm also allows for real-time step estimation for step sizes as small as 8 nm with dwell time of 5 ms or higher without sacrificing force regulation. © *2013 AIP Publishing LLC*. [http://dx.doi.org/10.1063/1.4824816]

Motor proteins such as kinesin and dynein are critical components of intracellular transport. Their study is important to understand cellular functionality, where malfunction in their transport may cause neuro-degenerative diseases such as Alzheimer's.[1,2] Optical traps provide an efficient way of probing the motor proteins via bead handles as they enable nm spatial resolution and fN force resolution capabilities.[3] Challenge in furthering the interrogative capabilities of optical tweezer based studies of motor-proteins stem from the significant impact of thermal noise and the nonlinear dynamics of the system.

In an optical trap based interrogation system, polystyrene beads are attached to motor proteins which are then probed by the laser trap (see Figure 1). When the motor-protein takes a step on the microtubule (where the position of the motor-protein on the microtubule is denoted by x_m), the resulting extension of the stalk exerts a force on the polystyrene bead which in turn displaces the bead from the trap center x_T. The trap exerts a restoring force towards the trap center. Here, equilibrium position of the bead x_b is determined by the balance of the trap force (proportional to $x_T - x_b$) and the force exerted by the motor protein (proportional to x_b–x_m) (see Figure 1). For small displacements, force-displacement relationships above admit a linear Hookean spring approximation.[4]

One of the main objectives in the study of motor protein is to detect the stepping motion x_m. The major impediments in estimating the stepping motion accurately are the nonlinear force-extension relationship of the motor proteins, and the large influence of thermal noise on the bead. Constant force clamps[4,5] are designed to make the bead follow the protein motion by regulating x_b–x_T to a desired constant value. The efficacy of this method depends on the *disturbance rejection bandwidth* (the disturbance in this case being the motor stepping motion x_m), that is, how fast the effects of the protein motion are countered to maintain a constant trapping force. However, the state-of-the-art force clamps have low bandwidths. Therefore, they are effective only for slow stepping motions[4,5] and fail to regulate the trapping force when the protein is moving at a much higher speed (elaborated later). Passive clamps have been used to increase bandwidth, however, they are not suitable for probing fast moving motor proteins due to reduced trapping force[6] and limited extent of constant force region.[7]

The speed limitations in active clamps primarily arise due to the dynamics of the actuators that manipulate the trap position. In existing force clamp designs, the latencies caused by the physics of the actuators are not modeled appropriately, which forms one of the primary causes for limited speeds of operation of these designs. In an acousto-optic deflector (AOD) (which is typically used to manipulate trap position in state-of-the-art optical trapping systems), a diffraction grating is created by propagating sound waves through a crystal. The frequency of the sound wave is controlled by an input radio frequency (RF) wave. The first

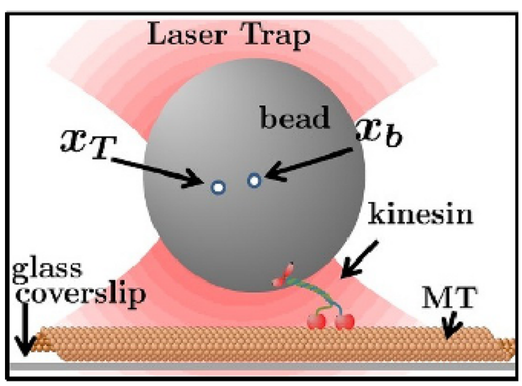

FIG. 1. A high resolution method to study kinesin motion is to optically trap the cargo (the bead) carried by the kinesin while it walks on microtubule. The bead position x_b is changed in response to the change in trap position x_T and the force exerted by the kinesin as it moves.

a)murtis@umn.edu and nanodynamics.ece.umn.edu

order diffracted spot created by passing a laser through this grating contains the majority of the light and is used to create a trap. The trap position can be manipulated by altering the input RF frequency, which affects the spacing of the grating caused by a change in the frequency of the sound wave traveling through the crystal. Here, the position of the laser spot at the output of the AOD does not settle until the propagating sound wave has crossed the entire width of the laser beam. Thus, the limitation in response time of the desired change in the trap location is determined by the velocity of the sound wave traveling in the crystal and the diameter of the laser beam. Another significant issue is caused by the partial reflection of the sound waves at the crystal boundaries. When the input frequency is changed, a mixture of waves of different frequencies exists in the crystal till the reflected waves die out completely. Thus, the time taken by the trap position to settle to its commanded position also depends on how well the sound waves get absorbed at crystal boundaries and the time taken by the reflected waves to die out.[8]

In this work, we incorporate models of components of the optical trapping system (including the AOD) into the design. Here the trap location x_T manipulable via the AOD exerts a trapping force depending on $x_T - x_b$, x_b being the bead position which is sensed by a photosensitive detector (PSD). Figures 2(a)–2(c) illustrate the responses of a bead in a trap when the AOD is actuated with known signals. Figure 2(a) shows the amplification in the amplitude of the sinusoidal bead motion (as measured by the PSD) obtained when

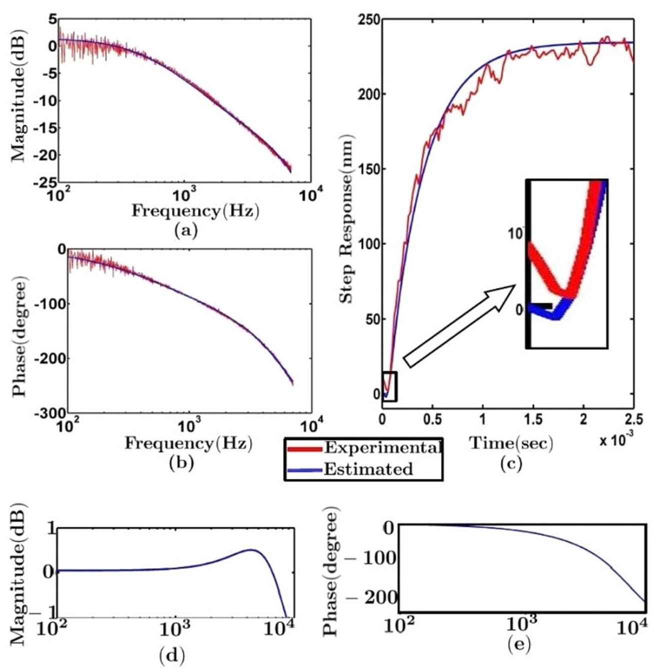

FIG. 2. The characterization of the system by frequency sweep method is demonstrated here. The red plots in (a) and (b) shows the experimentally obtained magnitude and phase response of the system while the blue curve corresponds to the transfer function fit of the same. (c) validates the estimated transfer function by comparing the simulated step response with the estimated transfer function (blue) with that obtained experimentally. The initial negative kick present in both the experimental and simulated step response (shown inset) is a signature of the delay present in the actuator. (d) and (e) show the magnitude and phase response of the instrument dynamics, respectively, which is extracted from the estimated transfer function and using estimated values for viscous drag coefficient and trap stiffness.

the AOD is commanded to change the trap location sinusoidally over a range of frequencies. Here, the phase shown in Figure 2(b) is the phase lag of the response sinusoid with respect to the command sinusoid provided to the AOD. This frequency response data can be used to obtain the *transfer function* (Laplace domain input-output relationship that describes the dynamic relationship between the actuation input to the AOD and the PSD measurement).[9] As alluded to earlier, the AOD physics describing the latencies can be quite complicated. However, the model of the AOD obtained using the experimentally obtained frequency response is accurate; indeed, as is evident from Figure 2(c), for the AOD and the experimentally obtained responses when the trap location is commanded to change by a step, quantitatively matches the response predicted by the model. It is also evident from the inset in Figure 2(c) that the bead initially moves in a direction opposite to the commanded direction which is a signature of delays present in the system.[9] Such behavior cannot be explained by the spring-mass-damper[3,4] models typically used to describe trap dynamics alone (see supplementary material text for more details). The transfer function $D(s)$ from the trap movement command u, provided as an input to the AOD, and the actual trap movement x_T, is determined to be $D(s) = \frac{0.66(s^2 - 7.98\times10^4 s + 2.78\times10^9)}{s^2 + 5.51\times10^4 s + 1.81\times10^9}$ (also see supplementary material text for details). The corresponding frequency response $D(j\omega)$ is shown in Figures 2(d) and 2(e), which is obtained by setting $s = j\omega$ at various angular frequencies ω. $|D(j\omega)|$ signifies the amplification and $\tan^{-1} D(j\omega)$ signifies the phase lag from input to output for an input sine-wave of frequency ω. It can be seen that as the phase lag becomes significant at higher frequencies, the assumption that trap position moves instantaneously in response to the input command (or, in other words $D(s)$ can be treated as unity) remains valid only for low frequencies. Violation of this assumption would not only prevent from achieving desired performance at higher frequencies, but may introduce instability in the system as well.[7]

We emphasize that unlike current works, it is not assumed that the trap position x_T is manipulable directly. However, as we have modeled the AOD dynamics, the trap position x_T can be estimated from the trap command u using the model $D(s)$. For slow stepping motion, the disturbance effects on the trap are predominantly in the low frequency and therefore approximating $D(s)$ by unity (and thus $u = x_T$) is valid whereas for fast stepping motion it is not. For fast stepping motion, $x_T \neq u$ and thus the error in force regulation $e_f = f_d - k_T(x_b - x_T)$ (where f_d is the desired force to be maintained and k_T is the stiffness of the trap) cannot be directly estimated, rendering active force clamps which depend on error e_f ineffective for high bandwidth studies. To circumvent this issue, in this letter we provide a method that does not rely on the regulated variables (such as e_f) to be measurable to achieve the goals of regulating a constant trapping force.

As mentioned before, one of the main objectives of force regulation is to allow for the estimation of the motor protein stepping motion accurately. In our method, it is possible to pose the estimation of stepping motion as the primary objective, with force regulation and reduction of noise on the estimate as secondary objectives. The high magnitude of thermal noise affecting the bead (whose standard deviation is comparable to the step sizes to be estimated) makes real time estimation of steps challenging. Long time averaging can be employed; however it is limited to stepping motion of frequency 1 Hz or less.[10] The effect of thermal noise can be reduced by making the system stiffer, which has the adverse effect of reducing the sensitivity of the system. We here provide an approach to reduce the effect of thermal noise on the stepping motion estimate without reducing the sensitivity of the system to the stepping motion.

Figure 3 provides a block diagram view of the framework where blocks in the figure represent transfer functions. The bead position x_b is fed back to the controller K along with the desired force command f_d, which then generates the command u to move the trap position x_T. The controller, unlike in traditional schemes, also provides an estimate $\hat{x}_m$ for the stepping motion x_m. We use the notation $T_{ab}(s)$ and $T_{ab}(j\omega)$ to denote the transfer function and the frequency response from an input a to an output b, respectively. Also, we use the notation $\| T_{ab}\|_\infty = \max_\omega |T_{ab}(j\omega)|$ to denote the maximum amplification from a to b over all frequencies and $\| T_{ab}\|_2 = (\frac{1}{2\pi}\int_0^\infty |T_{ab}(j\omega)|^2 d\omega)^{\frac{1}{2}}$ to denote the *rms* of the output b due to a white noise input a. The objective of force regulation, which requires that the error in force regulation e_f due to the disturbance (the stepping motion x_m) to be constrained below a pre-specified level γ_f for all frequencies, can be specified as $\| T_{x_m e_f}\|_\infty < \gamma_f$. Similarly, the objective of step estimation can be written as $\| T_{x_m \tilde{x}_m}\|_\infty < \gamma_m$, where $\tilde{x}_m = x_m - \hat{x}_m$ is the error in the estimate of step $\hat{x}_m$. A third objective $\| T_{\eta \hat{x}_m}\|_2 < \nu_m$ is introduced to reduce the effect of thermal noise on the estimate $\hat{x}_m$.

Weighting functions, denoted by blue dashed boxes in Figure 3, allow for the specification of frequency ranges in which a certain objective needs to be achieved. Appropriate selection of weighting function also ensures varying degrees of emphasis on different objectives. Once the problem is cast in the framework mentioned above, solution of the related optimization problem[11,12] yields a controller that meets the specified design requirements with guaranteed performance limits set by γ_f, γ_m, and ν_m. Note that the underlying optimization problem is a non-convex one and is a hard problem to solve. We apply the transformations mentioned in Refs. 11 and 12 to map it into an equivalent convex optimization problem, whose solution can be obtained by solving a set of linear matrix inequalities. The details of the methodology can be found in the supplementary material text. We mention here that if the design requirements become too stringent, the solution to the related optimization problem becomes infeasible. Relaxation of constraints is then required by changing the weighting functions and the performances limits to make the problem feasible. For details of the control system design, please refer to the supplementary material text.[16]

For experimental studies, we employed optical tweezers with a trap stiffness of $k_T = 0.015$ pN/nm and a bead with drag coefficient $\beta = 1.7 \times 10^{-5}$ pN s/nm. The desired force to be maintained, f_d, is set at 2.4 pN. The disturbance simulating the motor stepping motion is realized for an effective motor stiffness of $k_m = 0.3$ pN/nm. The motor stepping motion is simulated by giving square pulse disturbances with 50% duty cycle with a time period which is double the intended dwell time of the stepping motion. The estimated $D(s)$ is used to compute x_T from u in the analysis below. Using a dedicated field programmable gate array (FPGA) to implement the controller, a loop closure rate of 100 kHz (significantly faster than existing force clamps[4,5] where this is less than 1 kHz) was achieved, which is critical in achieving the desired performance.

Histograms in Figures 4(a) and 4(b) show the quality of the force regulations achieved against simulated motor velocities of 400 nm/s and 10 μm/s, respectively, where the control scheme[5] ignores the AOD dynamics (or in other words, assumes $D(s) = 1$) and updates the trap position as $u = x_{bf} - x_{bT}$, where x_{bf} is the filtered version of x_b and x_{bT} is the desired distance to be maintained between the trap and the bead center. The bead position x_b is filtered to minimize the high frequency noise, so that the assumption $u = x_T$ (or $D(s) = 1$) remains valid. It is evident from the figure that the above scheme is limited for force regulation on motor

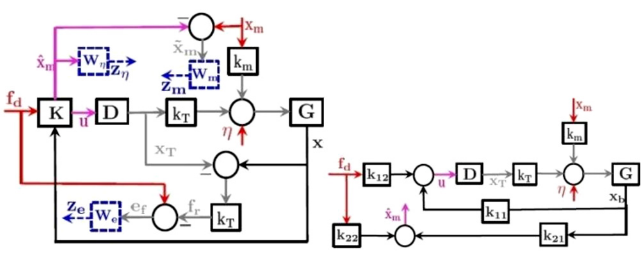

FIG. 3. Block diagram on the left hand elaborating the modern controller design paradigm. Red signals denote system inputs (commands or disturbances), magenta signals denote controller outputs, black signals denote the observable signals while the grey signals denote the unobservable ones. Blue boxes denote the weighting functions that capture the performance specifications, and the corresponding blue signals are fictitious signals introduced during the design phase to meet various design objectives. Here, the aim is to obtain an estimate $\hat{x}_m$ of motor motion x_m, with small influence of the thermal noise η on the estimate $\hat{x}_m$, while maintaining the force f_r on the motor regulated at a desired value f_d. Here G denotes the plant transfer function, D denotes the AOD transfer function (the variable s in dropped for notation convenience), k_T and k_m denote the trap and (simulated) motor stiffness, respectively. The weighting functions $W_e(s)$, $W_\eta(s)$, and $W_m(s)$ capture the objectives of force regulation (e_f being the error between desired and achieved load force), limiting the effect of thermal noise on stepping motion estimate and step estimation bandwidth, respectively. The right hand block diagram shows the control architecture and the different filters embedded in the controller K. k_{11} and k_{12} produce the control signal for force regulation while k_{21} and k_{22} generate the estimate of motor stepping motion.

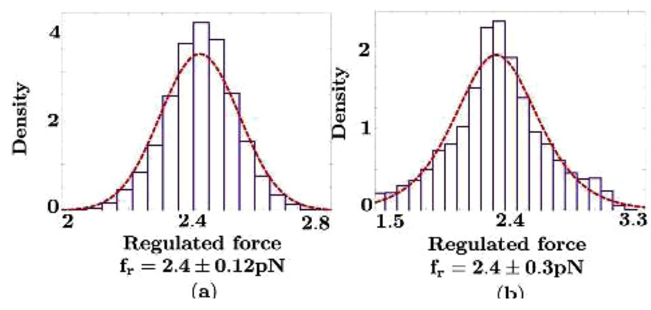

FIG. 4. Histograms showing the force regulation achieved with a traditional control scheme for different square pulse disturbances: (a) amplitude 8 nm and dwell time 20 ms, which corresponds to a motor velocity of 400 nm/s and (b) amplitude 25 nm and dwell time 2.5 ms, which corresponds to a motor velocity of 10 μm/s. It can be seen from the histograms that the controller maintains the force within 5% of desired value for lower motor velocity whereas the regulation deteriorates (12.5%) for higher motor velocity.

proteins moving slowly (400 nm/s, similar to what is achieved in Ref. 5) but not on motor proteins moving at significantly higher velocities (10 μ/s).

Histograms in Figures 5(a) and 5(b) show the force regulations achieved for the same simulated motor velocities as in the previous case with an optimal controller designed following our method which incorporates the estimated $D(s)$, where the only objective is force regulation. Here, the controller is suitable for force regulation on motor proteins moving at velocities that are an order of magnitude or more than achieved in Refs. 4 and 5. The limitation on achievable bandwidth is now caused by the bead-handle dynamics (how fast the bead can respond to the motor motion), which is common to all active as well as passive clamps. Clearly, the limitations of low disturbance rejection bandwidth and instability about feedback based force clamps, as mentioned in Ref. 7 can be overcome. Another limitation arises due to the presence of right half plane zeros in the AOD dynamics (see $D(s)$), which poses a fundamental limit on the achievable performance.[13]

Figures 6(a) and 6(b) demonstrate the *real-time* step estimation capability achieved by our method while Figures 6(e) and 6(f) show that corresponding force regulations are within satisfactory limit so that bead displacement can be used to infer motor motion without the need for linkage corrections.[4] The corresponding noisy bead position traces are shown in Figures 6(c) and 6(d) from which the steps are typically estimated offline.

Small error in estimating the stepping motion (that is small $\| T_{x_m\tilde{x}_m}\|_\infty$) requires the transfer function $T_{x_m\tilde{x}_m}$ from the actual to the estimated motion be such that $|T_{x_m\hat{x}_m}(j\omega)| \approx 1$ for the range of frequency of interest Ω_r. This would, however, increase the effect of thermal noise on the estimate $\| T_{\eta\hat{x}_m}\|_2$ where noise is integrated over Ω_r, since $|T_{\eta\hat{x}_m}| = \frac{1}{k_m}|T_{x_m\hat{x}_m}|$. Thus, from practical considerations, Ω_r needs to be chosen carefully so that we achieve satisfactory noise reduction at the step estimate $\hat{x}_m$ along with step estimation in the desired frequency range. This also explains why the noise level increases as we increase the bandwidth of step estimation.

To summarize, in this letter, we have precisely characterized the instrument dynamics and adopted a model based modern control paradigm[11] to design an active force clamp that is capable of probing motor proteins with satisfactory force regulation close to their native cellular environment (where vesicles are transported at close to 4 μm/s) (Ref. 14) and also motor proteins having larger step sizes and hence higher velocities (such as ciliary dynein with velocities close to 7 μm/s).[15] This is much higher than the state-of-the-art capability[5] shown to operate satisfactorily on kinesin moving at velocities up to 450 nm/s. Simultaneously, this paradigm allows for estimation of motor stepping motion in real-time for high motor velocities (more than what is achieved for kinesin *in vitro*[14]). We demonstrated estimation of square pulses of magnitude as small as 8 nm with dwell time of 5 ms, without sacrificing the force regulation. Although long time averaging and median filtering is employed[10] to estimate steps in real time, it is limited to the cases with dwell time between steps of 1 s or higher, thus rendering them unsuitable for motor protein related applications. Thus the approach discussed here enables exploration of spatial and temporal realms of motor protein investigation which are not currently possible.

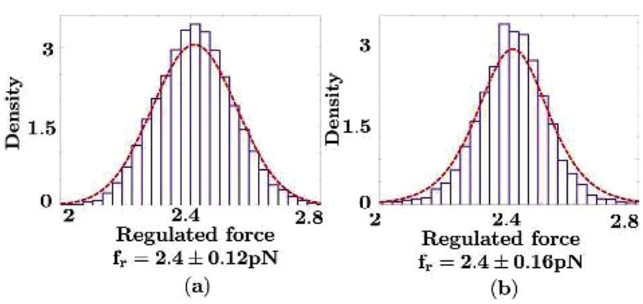

FIG. 5. Histograms showing the force regulation achieved with an *optimal* controller with the only objective of force regulation for different square pulse disturbances: (a) amplitude 8 nm and dwell time 20 ms, which corresponds to a motor velocity of 400 nm/s and (b) amplitude 25 nm and dwell time 2.5 ms, which corresponds to a motor velocity of 10 μm/s. It is evident from the histograms that the controller maintains the force within 6.7% of desired value even for high frequency high magnitude disturbances (higher velocity).

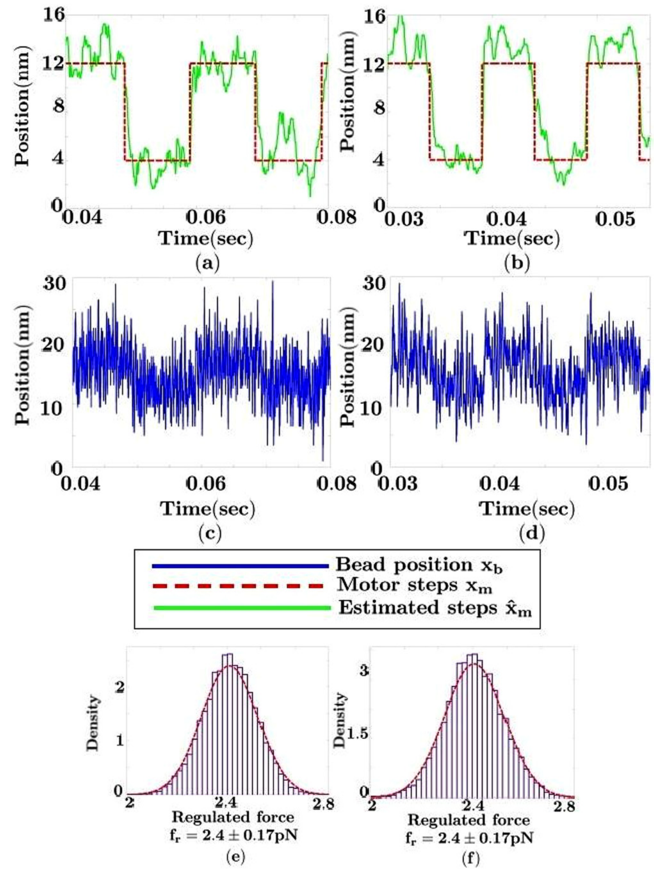

FIG. 6. The real time step estimation for step size 8 nm is demonstrated for (a) dwell time 10 ms, which corresponds to a motor velocity 800 nm/s and (b) dwell time 5 ms, which corresponds to a motor velocity 1600 nm/s. (c) and (d) show the corresponding noisy bead position measurements, from which the steps are typically estimated via post-processing, while (e) and (f) show the corresponding force regulation achieved.

This research was supported by NSF grant award No. ECCS 1202411.

[1]N. Hirokawa, Y. Noda, Y. Tanaka, and S. Niwa, Nat. Rev. Mol. Cell Biol. **10**, 682 (2009).

[2]G. B. Stokin, C. Lillo, T. L. Falzone, R. G. Brusch, E. Rockenstein, S. L. Mount, R. Raman, P. Davies, E. Masliah, D. S. Williams *et al.*, Science **307**, 1282 (2005).
[3]W. J. Greenleaf, M. T. Woodside, and S. M. Block, Annu. Rev. Biophys. Biomol. Struct. **36**, 171 (2007).
[4]K. Visscher and S. M. Block, Methods Enzymol. **298**, 460 (1998).
[5]M. J. Lang, C. L. Asbury, J. W. Shaevitz, and S. M. Block, Biophys. J. **83**, 491 (2002).
[6]R. Nambiar, A. Gajraj, and J.-C. Meiners, Biophys. J. **87**, 1972 (2004).
[7]W. J. Greenleaf, M. T. Woodside, E. A. Abbondanzieri, and S. M. Block, Phys. Rev. Lett. **95**, 208102 (2005).
[8]A. Knight, G. Mashanov, and J. Molloy, Eur. Biophys. J. **35**, 89 (2005).
[9]K. Ogata, *Modern Control Engineering*, 5th ed. (Prentice-Hall, Upper Saddle River, NJ, USA, 2010).
[10]E. A. Abbondanzieri, W. J. Greenleaf, J. W. Shaevitz, R. Landick, and S. M. Block, Nature **438**, 460 (2005).
[11]C. Scherer, P. Gahinet, and M. Chilali, IEEE Trans. Autom. Control **42**, 896 (1997).
[12]C. Lee and S. Salapaka, IEEE/ASME Trans. Mechatron. **14**, 414 (2009).
[13]T. Aggarwal, H. Sehgal, and M. Salapaka, Rev. Sci. Instrum. **82**, 115108 (2011).
[14]J. Gagliano, M. Walb, B. Blaker, J. C. Macosko, and G. Holzwarth, Eur. Biophys. J. **39**, 801 (2010).
[15]R. D. Vale, F. Malik, and D. Brown, J. Cell Biol. **119**, 1589 (1992).
[16]See supplementary material at http://dx.doi.org/10.1063/1.4824816 for detailed description of experimental setup, system model, experimental realization of stepping motion, and control system design.